Bull. Mater. Sci. (2020) 43:315
https://doi.org/10.1007/s12034-020-02285-2

Enhancement of thermoelectric performance of *n*-type $AgBi_{1+x}Se_2$ via improvement of the carrier mobility by modulation doping

EKASHMI RATHORE†, SATYA N GUIN† and KANISHKA BISWAS*
New Chemistry Unit, School of Advanced Materials and International Centre for Materials Science, Jawaharlal Nehru Centre for Advanced Scientific Research, Bangalore 560064, India
*Author for correspondence (kanishka@jncasr.ac.in)

MS received 20 February 2020; accepted 13 July 2020; published online 14 December 2020

Abstract. High charge carrier mobility with low lattice thermal conductivity is one of the key factors for the design of a good thermoelectric material. Recent studies show that *n*-type Te-free $AgBiSe_2$ is promising compound for thermoelectric energy conversion due to intrinsically low lattice thermal conductivity. However, low charge carrier mobility in $AgBiSe_2$ is the constraint for enhancement of its power factor. In the present study, we use a chemical modification way to realize modulation doping in $AgBiSe_2$. The addition of 2–6 mol% excess Bi in $AgBiSe_2$ results in the formation of Bi-rich modulation-doped microstructures of topological semimetal, Bi_4Se_3 in $AgBiSe_2$ matrix. We show that due to facile carrier transport via semi-metallic Bi_4Se_3 microstructure results in overall improvement of carrier mobility without compromising Seebeck coefficient in $AgBiSe_2$ system, which in turn results in a remarkable improvement in the power factor (σS^2) value. A highest σS^2 value of $\sim$6.35 μW cm^{-1} K^{-2} at 800 K has been achieved in $AgBiSe_2$-3% Bi excess sample, which is higher than previously reported metal ion and halogen-doped $AgBiSe_2$.

Keywords. Thermoelectrics; modulation doping; mobility; power factor; thermal conductivity.

1. Introduction

In the recent years, the energy and environment related concern intensified the research in the arena of efficient, cost-effective and pollution-free means of power generation. Thermoelectric materials are the all solid-state converters without any moving part, can directly and reversibly convert waste heat into electricity [1–4]. Over the last two decades, there has been an escalated interest in the field of thermoelectric materials research. The effectiveness of a thermoelectric material is governed by the thermoelectric figure of merit, $zT = \sigma S^2 T/\kappa$, where σ is the electrical conductivity, S is the Seebeck coefficient, T is the temperature in Kelvin and κ is the thermal conductivity [1–4]. The fundamental challenge to design a promising thermoelectric material is intriguing due to conflicting thermoelectric parameters. To improve the thermoelectric properties, different concepts have been employed via improvement of the Seebeck coefficient or reduction of the thermal conductivity or by simultaneous tailoring of both the parameters. The Seebeck coefficient can be improved by the introduction of resonant levels in the electronic structure or by electronic band convergence [5,6]. On the other hand, κ_{lat} can be reduced by solid solution alloying, nanostructuring and all-scale hierarchical structuring [3,7,8]. The inorganic solids with intrinsically low κ_{lat} [9] due to rattling modes [10], soft phonon modes [11–13], resonant bonding [14] and high lattice anharmonicity [15] are realized recently to be promising candidates for the thermoelectric application.

Among the intrinsically low κ_{lat} compounds, the copper- and silver-based Te-free I–V–VI_2 (where I = Cu, Ag or an alkali metal; V = Sb, Bi; and VI = S, Se) chalcogenide semiconductors have shown promise for enhanced thermoelectric properties [16–22]. The multiple soft phonon modes and strong phonon–phonon interaction caused by large bonding anharmonicity due to repulsion between the ns^2 lone pair of group V elements and valence p orbital of chalcogenide is the origin of high thermal resistance for these compounds [16]. In recent years, several new Te-free materials from this class have been discovered as potential candidate thermoelectrics. In the *p*-type family, $AgSbSe_2$ and in *n*-type family, $AgBiSe_2$ have established to be the most promising candidates [17,20,21,23,24]. At room temperature, $AgBiSe_2$ crystallizes in a cento-symmetric

†These authors contributed equally to this study.

This article is part of the Topical Collection: SAMat Focus Issue.

Electronic supplementary material: The online version of this article (https://doi.org/10.1007/s12034-020-02285-2) contains supplementary material, which is available to authorized users.

cation-ordered hexagonal structure with space group *P*-3*m*1 and lattice parameter a = 4.194 Å, c = 19.65 Å [25]. It shows two structural transitions at higher temperature. The hexagonal (α) to rhombohedral (β) (space group *R*-3*m*, a = 7.022 Å) transition takes place at ∼460 K (figure 1). During α–β transition, the cation sublattice remains ordered, but a slight atomic displacement and an elongation of the unit cell in the (001) direction of the hexagonal lattice take place. The ordered rhombohedral (β) to cation-disordered cubic (γ) (space group *Fm*-3*m*, a = 5.832 Å) phase transition takes place at ∼580 K [25].

Although pristine $AgBiSe_2$ exhibits low thermal conductivity, its thermoelectric performance is poor due to low electrical transport [20]. The thermoelectric property of $AgBiSe_2$ has been improved by regulating carrier concentration, using electron doping strategy in host cationic or anionic site. For instance, solid solution alloying of higher valent cation (Nb, In or Ge) in the Ag site, optimizes the *n*-type carrier concentration and leads to enhancements of zT [20,26,27]. The doping of monovalent halide ion (Cl^-/Br^-/I^-) on the divalent selenium (Se^{2-}) site can act as an *n*-type dopant in $AgBiSe_2$ and results in the significant improvement in thermoelectric properties [21]. Furthermore, the effect of Ag vacancy defect and tellurium substitution on the transport property of $AgBiSe_2$ has been investigated [28,29]. However, low carrier mobility for pristine $AgBiSe_2$ (∼67 $cm^2\ V^{-1}\ s^{-1}$) and doped samples still restrict to improve the electrical transport properties.

Generally, in heavily doped semiconductors, the high population of free carriers leads to a diminution of carrier mobility due to increased carrier–carrier scattering and ionized impurity scattering [1]. Recently, the concept of three-dimensional (3D) modulation doping (MD) has been introduced to improve the carrier mobility in thermoelectric materials [1,22,30]. Usually, modulation-doped samples are a physical mixture of two-phase composites made of undoped and heavily doped counterparts. The undoped counterpart has low carrier concentration, but high carrier mobilities, whereas the doped counterpart has high carrier concentrations, but low carrier mobilities. In a heavily doped semiconductor, the high population of free carriers can spill over throughout the matrix. However, in a modulation-doped sample, one can force the charge carriers to spill over from the modulation-doped region into the surrounding host matrix. Therefore, the ionized atoms remain spatially separated within the modulation-doped region. Consequently, the ionized impurity scattering rate can be decreased in modulation-doped sample and an overall improvement of carrier mobility can be achieved [22,30–32]. Historically, this technique was first implemented in two-dimensional electron gas (2DEG) thin film devices for improving the carrier mobility and thus, the electrical conductivity [33]. In thermoelectrics, using modulation doping, enhanced power factor was achieved in $Si_{1-x}Ge_x$ composites by mechanically mixing the doped and undoped $Si_{1-x}Ge_x$ nanograins [32]. The concept of modulation doping is successfully applied to BiCuSeO [30], BiAgSeS [22] and half-Heusler TiNiSn [33]. All these reports encouraged us to investigate the MD approach in intrinsically low thermal conductivity $AgBiSe_2$ system where electronic transport can be improved by enhancing the carrier mobility.

Herein, we report a large enhancement of power factor in $AgBiSe_2$ by enhancing carrier mobility by modulation doping. The present modulation doping is quite different from the conventional approach. In our study, we have used 2–6 mol% excess Bi as a modulation dopant in $AgBiSe_2$ to improve the carrier transport. We demonstrate a chemical modification way to realize modulation doping in $AgBiSe_2$ by embedding bismuth-rich microstructure in $AgBiSe_2$ matrix through matrix encapsulation technique. We have chosen Bi for two reasons. Firstly, Bi is an *n*-type semimetal with a small Fermi surface (low carrier effective mass), long carrier mean free path and extremely high electron mobility (∼10^4 $cm^2\ V^{-1}\ s^{-1}$ at 300 K) [34]. Secondly, Bi is a constitute element of $AgBiSe_2$ and therefore, it ruled out the aliovalent doping in the parent $AgBiSe_2$ phase and minimizes the possibility of ionized impurity scattering process. The diffusion of electrons from $AgBiSe_2$ matrix to Bi-rich semi-metallic precipitate results in an overall enhancement of carrier mobility in $AgBiSe_2$-x% Bi (x = 2–6 mol%) system. We show that the addition of small fraction of Bi in $AgBiSe_2$ results in a large effect on the microstructure and transport properties of $AgBiSe_2$. PXRD and microstructure analysis reveals that $AgBiSe_2$-x% Bi samples are not single phase, but rather forms a microstructure composed of well dispersed Bi-rich nano/micro-inclusion of topological semimetal, Bi_4Se_3 [35,36] in the matrix of $AgBiSe_2$. Electrical transport measurement shows that the MD approach enhances the carrier mobility and hence, electrical conductivity in $AgBiSe_2$ which results in a remarkable improvement in the power factor (σS^2) value over wide temperatures. A maximum power factor value of ∼6.35 μW $cm^{-1}\ K^{-2}$ at 800 K was measured in $AgBiSe_2$-3% Bi, which is higher than the metal ion and halogen-doped $AgBiSe_2$ system.

2. Experimental

Ingots (∼7 g) of pristine $AgBiSe_2$ and $AgBi_{1+x}Se_2$ (x = 2–6 mol%) were synthesized by melting reaction of stoichiometric amounts of high-purity elemental silver (Ag, 99.9999%, metal basis, Alfa Aesar), elemental bismuth (Bi, 99.9999%, metal basis, Alfa Aesar) and elemental selenium (Se, 99.999%, metal basis, Alfa Aesar), taken in quartz tubes which were sealed under high vacuum (∼10^{-5} Torr). The sealed tubes were slowly heated up to 723 K in 12 h, then heated up to 1123 K in 4 h, soaked for 10 h, and eventually slow-cooled to room temperature over a period of 12 h. For transport property measurements, the samples were cut using a low-speed diamond saw and polished using

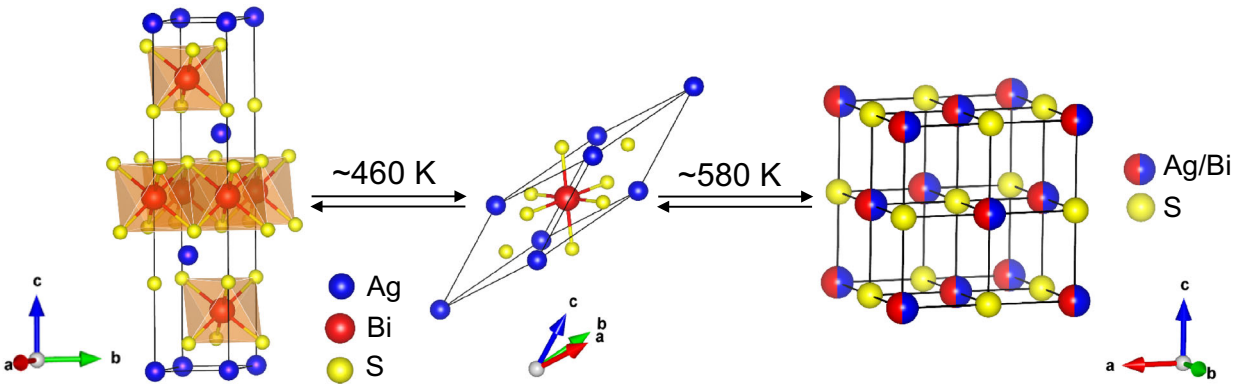

Figure 1. Temperature-dependent structural phase transitions in $AgBiSe_2$. The room-temperature hexagonal and the intermediate rhombohedral phases are cation-ordered structure. The high-temperature cubic phase is a cation-disordered structure.

a polisher. Density of the samples was found to be ~97% of the theoretical value of pristine $AgBiSe_2$. Powder X-ray diffraction patterns (PXRD) for finely powder samples were recorded using a CuKα (λ = 1.5406 Å) radiation source on a Bruker D8 diffractometer. The room temperature carrier concentration of the samples was determined by Hall coefficient measurement system using a home-build measurements system. FESEM images were derived using NOVA NANO SEM 600 (FEI, Germany) operated at 15 kV. Electrical conductivity and Seebeck coefficients were measured concurrently under a helium atmosphere from room temperature to ~823 K on a ULVAC RIKO ZEM-3 instrument system. The sample for the measurement is parallelepiped with dimensions of $\sim 2 \times 2 \times 8$ mm^3. The longer direction matches the direction in which the thermal conductivity was measured. Heating and cooling cycles gave repeatable electrical properties for a given sample. Electrical and thermal transports are measured in the same direction. The thermal diffusivity (D) was measured by laser flash method (Netzsch LFA-457) from room temperature to ~823 K. It was performed on carbon-coated disc samples of 8 mm in diameter and 2 mm thickness under an N_2 atmosphere. Temperature-dependent heat capacity, C_p, was derived using the standard sample (pyroceram) in LFA-457. Cowan model with pulse correction was used to analyse the thermal diffusivity data. The total thermal conductivity, κ_{total}, was estimated using the formula: $\kappa_{total} = DC_p\rho$, where ρ is the density.

3. Results and discussion

The crystalline ingots of $AgBiSe_2$ and $AgBiSe_2$-x% Bi (x = 2–6 mol%) were synthesized by elemental melting reaction in vacuum-sealed quartz tubes followed by slow cooling. Figure 2a shows PXRD pattern of pristine and $AgBiSe_2$-x% Bi samples. The pattern for pristine sample could be indexed based on hexagonal $AgBiSe_2$. The XRD patterns for Bi excess samples show additional reflections of the second phase of topological semimetal, Bi_4Se_3 (* marked in the plot). The intensity of the additional peaks increases with the rise in bismuth concentration which implies the increase in secondary phase of Bi_4Se_3 in the sample. Supplementary figure S1 shows that * peaks can be indexed to Bi_4Se_3 in 6% Bi-excess sample.

To confirm these extra reflections of secondary phase of Bi_4Se_3 in PXRD data, we have carried out backscattered electron imaging (BSE) during FESEM and energy dispersive X-ray spectroscopy (EDAX) to understand the microstructure in $AgBiSe_2$-x% Bi (x = 2–6 mol%). The BSE–FESEM image of 3% Bi modulation-doped sample is presented in figure 2b and c. The micrograph clearly shows two distinct regions with dark and bright contrasts. The elements with the higher atomic number has greater probability for elastic collision and looks brighter in BSE image. Thus, the region with bright contrast is related with heavier elements of the sample which is Bi_4Se_3 precipitates in the present case and EDAX analysis in supplementary figure S2b, confirms that the precipitates are Bi-rich phases, Bi_4Se_3. The darker contrast regions correspond to the matrix in supplementary figure S2a. To further evaluate the composition of the matrix and the precipitate, we have performed elemental line scanning which shows Bi-rich precipitate, while the matrix is close to the composition of $AgBiSe_2$. Thus, the microstructure analysis further confirms the presence of Bi-rich secondary phase of Bi_4Se_3 in the $AgBiSe_2$ sample.

In figure 3, we present temperature-dependent electronic transport properties of $AgBiSe_2$-x% Bi (x = 0–6 mol%). Pristine $AgBiSe_2$ exhibits a σ value of ~63 S cm^{-1} at room temperature (figure 3a, inset). The temperature-dependent, σ in the hexagonal phase maintains nearly constant value upto ~460 K. In the rhombohedral phase (temperature window of 460–580 K), the system exhibits metallic behaviour with σ drops from ~52 S cm^{-1} at 460 K to ~16 S cm^{-1} at 580 K. In the cubic phase (above ~585 K), the σ value increases to ~24 S cm^{-1} at 708 K. The σ value for Bi-modulation-doped samples is

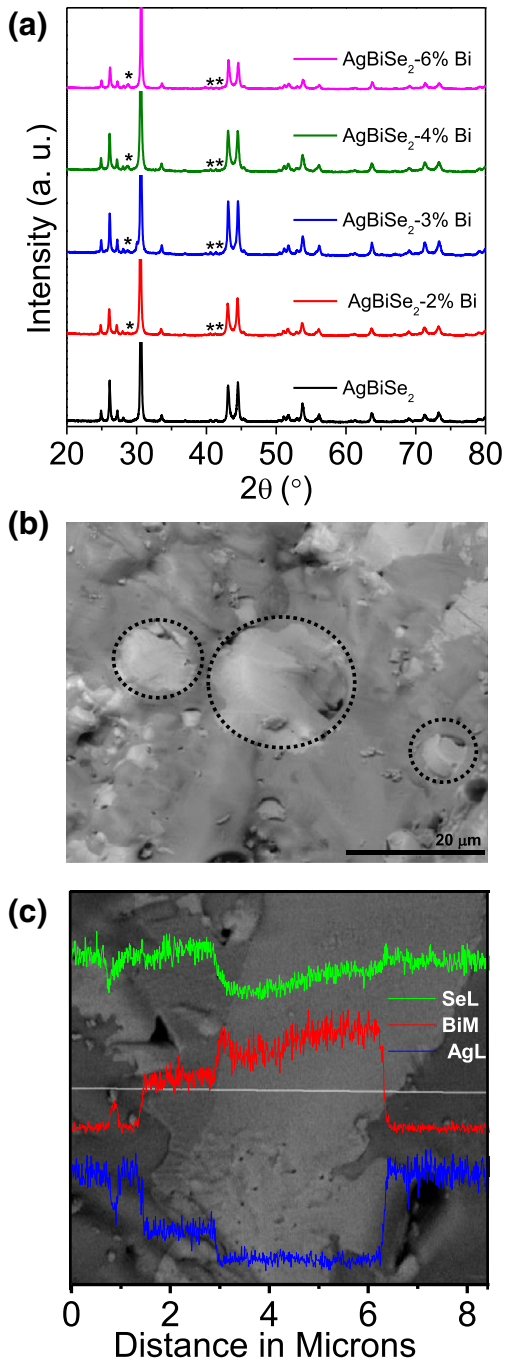

Figure 2. (**a**) Room temperature powder XRD pattern of pristine $AgBiSe_2$-x% Bi (x = 0–6 mol%) samples. * marks indicate extra reflection due to the second phase of Bi_4Se_3. (**b**) Backscattered FESEM image of the cleaved surface of $AgBiSe_2$-3% Bi sample, the Bi-rich precipitates with bright contrast is circled with black dotted line. (**c**) EDAX elemental line scan along the matrix and precipitate.

considerably higher than the pristine sample, which shows an increasing trend with rise in Bi concentration (figure 3a). The modulation-doped samples show a similar metal to semiconductor type transition during rhombohedral to cubic phase transformation like in pristine $AgBiSe_2$, which is also observed in metal ion and halogen-doped samples of $AgBiSe_2$ [20,21,26,27]. Typically, for $AgBiSe_2$-3% Bi sample, the σ value changes from $\sim$380 S cm^{-1} at room temperature to $\sim$435 S cm^{-1} at 800 K.

To get better insights for the improvement of the electrical conductivity value, we have measured carrier concentration of the selected samples. The negative value of Hall coefficient (R_H), at ambient temperature for pristine and $AgBiSe_2$-x% Bi (x = 0–6 mol%) samples indicates n-type conduction in the system. We have estimated the carrier concentration (n) and carrier mobility (μ) from the formula: $n = 1/eR_H$, and $\mu = \sigma/ne$, respectively, where e is the electronic charge. The electrical conductivity (σ) is related to n through the carrier mobility (μ) through the following expression:

$$\sigma = ne\mu, \tag{1}$$

μ relies on the additional conditions shown in equation (2)

$$\mu = \frac{e\tau}{m^*}, \tag{2}$$

where τ is the relaxation time and m^* the carrier's effective mass. Notably, in the halogen- and cation-doped $AgBiSe_2$, the improvement in the carrier transport primarily due to the rise of carrier concentration. The Bi incorporation results in a slight increase in carrier concentration, while the carrier mobility increases dramatically compared to pristine sample (table 1). Typically, for $AgBiSe_2$-3% Bi, μ shows a value of $\sim$248 cm^2 V^{-1} s^{-1}, which is much higher than previously reported cation- and anion-doped $AgBiSe_2$ samples ranging from $\sim$22 to $\sim$63 cm^2 V^{-1} s^{-1} with similar carrier concentration [20,21], indicating that modulation doping suppresses the ionized impurity scattering. In addition, the diffusion of electrons to Bi_4Se_3 precipitate, where carrier mobility is higher than $AgBiSe_2$ matrix results in an overall improvement of μ in the system.

Temperature-dependent Seebeck coefficient (S) of $AgBiSe_2$ and Bi modulation-doped samples has been presented in figure 3b. Typically, $AgBiSe_2$-3% Bi sample shows an S value of -82.5 μV K^{-1} at room temperature which reaches a value of -100 μV K^{-1} at 460 K within the hexagonal phase. After the hexagonal to rhombohedral phase-transition, the Seebeck coefficient shows an increasing trend and reaches a value of the maximum value of -160 μV K^{-1} at 560 K. In the cubic phase, the S value decreases and reaches -120 μV K^{-1} at 800 K. Although the trend of S in the present case of Bi-excess is similar to the metal ion and halogen-doped $AgBiSe_2$, the value of S is lower in the measured temperature range. To understand this, we have calculated carrier effective mass (m^*) assuming single parabolic band model with acoustic phonon scattering ($r = -1/2$). The details of equation for the calculation can be found in electronis supporting information. We have observed a large decrease of m^* compare to pristine sample (table 1). Besides, the m^* value ranging from 0.18 to 0.20 is much smaller than halogen-doped

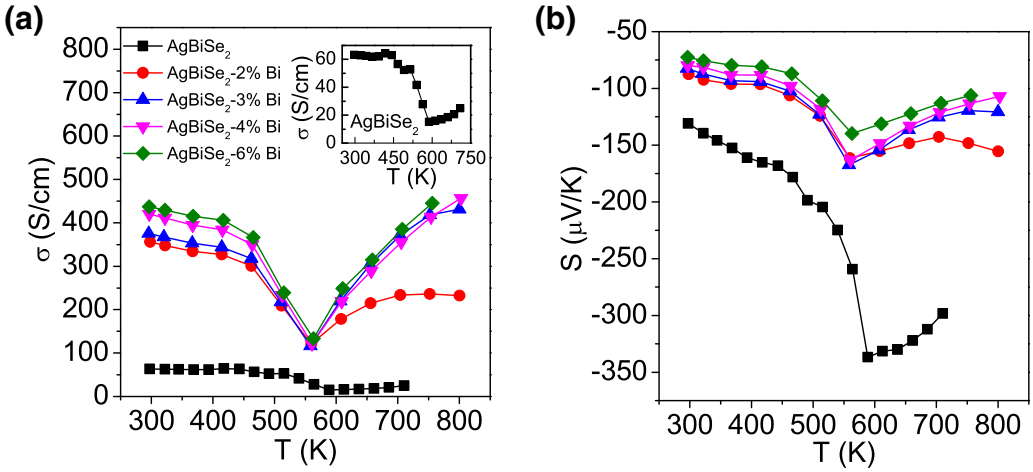

Figure 3. Temperature-dependent (**a**) electrical conductivity (σ) and (**b**) Seebeck coefficient (S) of $AgBiSe_2$-x% Bi (x = 0–6 mol%) samples. The inset in (**a**) shows zoomed data for pristine $AgBiSe_2$.

Table 1. Room temperature carrier concentration (n), electrical conductivity (σ), carrier mobility (μ) and effective mass (m^*) of $AgBiSe_2$-x% Bi (x= 0–6 mol%) samples.

Sample	n, cm^{-3}	σ, S cm^{-1}	μ, cm^2 V^{-1} s^{-1}	m^*/m_0
$AgBiSe_2$	5.85×10^{18}	63	67	0.25
$AgBiSe_2$-2% Bi	7.97×10^{18}	355	278	0.18
$AgBiSe_2$-3% Bi	9.46×10^{18}	375	248	0.19
$AgBiSe_2$-4% Bi	1.02×10^{19}	420	257	0.20
$AgBiSe_2$-6% Bi	1.52×10^{19}	437	180	0.19

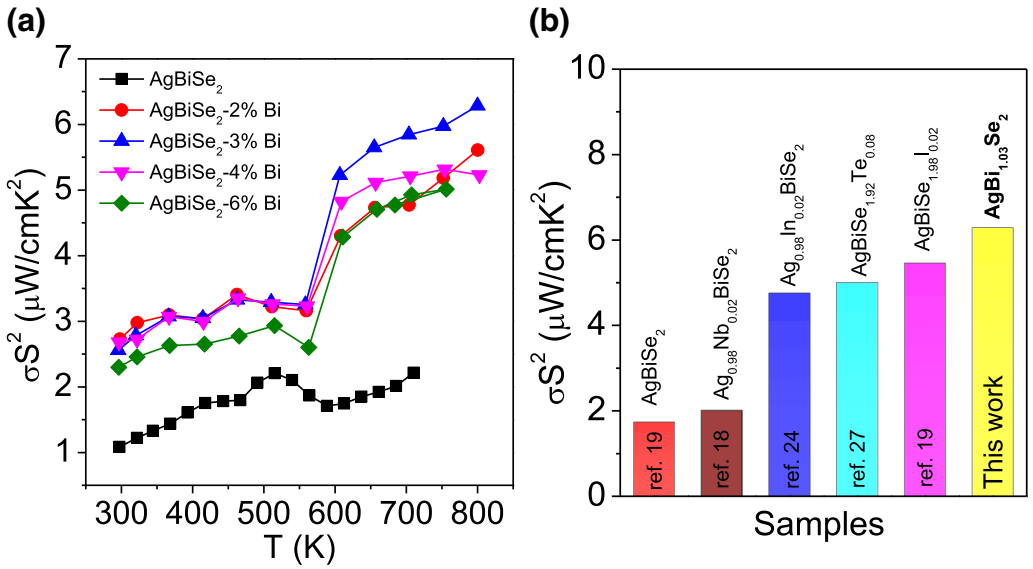

Figure 4. (**a**) Temperature-dependent power factor of (σS^2) $AgBiSe_2$-x% Bi (x = 0–6 mol%) samples and (**b**) comparison of power factors of the halogen- and metal ion-doped $AgBiSe_2$ samples.

samples with m^* ranging from 0.46 to 0.59 [21]. Thus, lower S value in the present case is due to a combined effect of decreased m^* and increase in the carrier concentration (n), as given by Mott equation, where S is directly proportional to the m^* ($S \sim m^*$) and inversely proportional to n ($S \sim n^{-2/3}$) [2]. We would also like to mention that low carrier effective mass (m^*) in the modulation-doped samples assists to increase overall carrier mobility

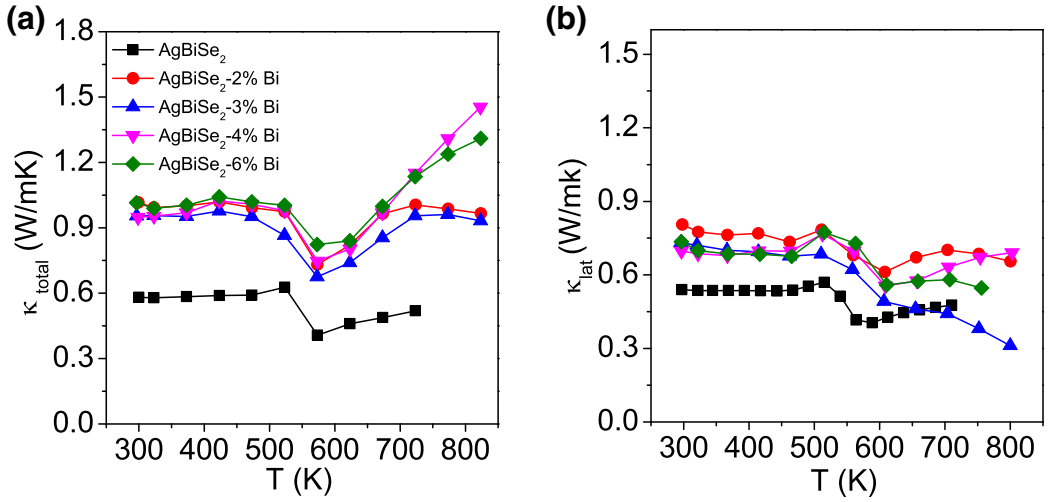

Figure 5. Temperature-dependent (**a**) total thermal conductivity (κ_{total}) and (**b**) lattice thermal conductivity (κ_{lat}) of $AgBiSe_2$-x% Bi (x = 0–6 mol%) samples.

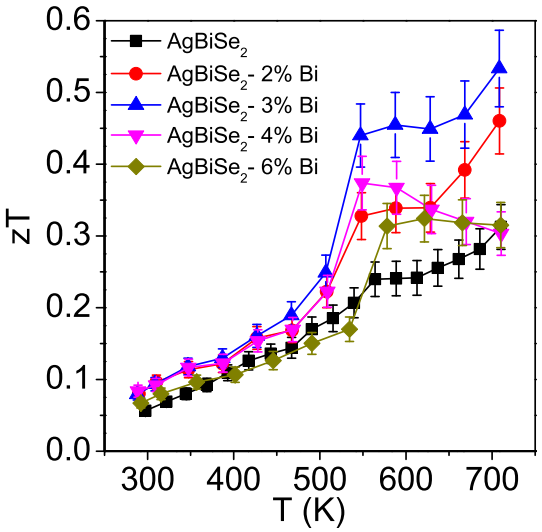

Figure 6. Temperature-dependent thermoelectric figure of merit (zT) of $AgBiSe_2$-x% Bi (x = 0–6 mol%) samples. 10% error bar has been shown in zT estimation.

(supplementary equation (S2)) which improve the σ in the present case.

The temperature-dependent power factor (σS^2) for all the samples, estimated from measured σ and S have been shown in figure 4a. The Bi modulation-doped samples show large improvement in σS^2 than the pristine sample. Typically, the $AgBiSe_2$-3% Bi sample shows a σS^2 of $\sim$2.6 μW cm^{-1} K^{-2} at room temperature which reaches a maximum value of $\sim$6.35 μW cm^{-1} K^{-2} at 800 K. Indeed, the maximum σS^2 value obtained in the present ingot samples is higher than that of the halogen- and metal ion-doped $AgBiSe_2$ ranging from $\sim$2.0 to $\sim$5.45 μW cm^{-1} K^{-2} (figure 4b) [20,21,26,29].

Figure 5a represent temperature-dependent total thermal conductivity, κ_{total}, of all the samples. κ_{total} has been estimated using the formula, $\kappa_{total} = DC_p\rho$, where D is the thermal diffusivity, C_p is specific heat and ρ is density of the sample (supplementary figure S3). All the doped samples show an increasing trend of κ_{total} over the measurement temperature. Typically, for $AgBiSe_2$-3% Bi sample, a κ_{total} of $\sim$0.95 W m^{-1} K^{-1} has been measured at room temperature, which decreases to a minimum value of $\sim$0.67 W m^{-1} K^{-1} in the rhombohedral at 570 K. With further increase in temperature in the cubic phase, the κ_{total} initially show an increasing trend and then reaches to a value of $\sim$0.93 W m^{-1} K^{-1} at 823 K. For higher concentration modulation-doped samples, $AgBiSe_2$-x% Bi (x = 4–6 mol%) in the cubic phase, the κ_{total} shows increasing trend. To understand this, we have extracted the contribution of lattice thermal conductivity (κ_{lat}) and electronic thermal conductivity (κ_{el}) (supplementary figure S4b) to the κ_{total} (figure 5b) using Wiedemann–Franz law: $\kappa_{el} = L\sigma T$, where L is the Lorenz number (supplementary figure S4a). L has been calculated using single parabolic band model, which can be found elsewhere [17]. The analysis indicates a large contribution from the κ_{el} at higher temperature results in such an observation. We also observed a small increase in κ_{lat} value in the modulation-doped sample compared to the pristine $AgBiSe_2$. Generally, in I–V–VI_2 family of compounds, the phononic contribution towards κ_{total} is already to a minimum value as the mean free path of the phonons is in the range of interatomic distance. Thus, the possibility of scattering of smaller mean free path phonons by the micrometer size precipitate can be ruled out here. We therefore, attribute that the increase in κ_{lat} might be associated with the additional contribution of κ_{lat} from the microstructure phase of Bi_4Se_3 which probably has higher thermal conductivity.

The estimated temperature-dependent thermoelectric figure of merit, zT from the electrical and thermal transport data for all the samples has been given in figure 6. The

estimation includes ∼10% error from the different measurement. The modulation-doped samples show higher zT value compared to pristine sample. The improvement in the zT value is due to large enhancement of electrical conductivity and power factor value due to improved carrier mobility of the sample. A highest zT value of ∼0.53 at 800 K has been achieved for $AgBiSe_2$-3% Bi sample.

4. Conclusions

In summary, our study shows that modulation doping is an effective way to improve carrier mobility in $AgBiSe_2$. We have shown that addition of small amount of Bi in $AgBiSe_2$ results in a large effect on the microstructure and transport properties of $AgBiSe_2$. The suppression of the ionized impurity scattering and injection of charge carrier to the precipitate of topological semimetal, Bi_4Se_3 from the $AgBiSe_2$ matrix result in the large improvement of carrier mobility. As a consequence, we have observed an increase in thermoelectric power factor and zT in $AgBiSe_2$. In general, low carrier mobility in I–V–VI_2 class of materials is constraint for the improvement of power factor. Our study demonstrates that use of heterogeneous modulation doping approach could be an effective strategy for improvement of carrier transport in I–V–VI_2 class of compounds.

Acknowledgements

This work was supported by New Chemistry Unit and Sheikh Saqr Laboratory, JNCASR.

References

[1] Tan G, Zhao L D and Kanatzidis M G 2016 *Chem. Rev.* **116** 12123
[2] Sootsman J R, Chung D Y and Kanatzidis M G 2009 *Angew. Chem. Int. Ed.* **48** 8616
[3] Zhao L D, Dravid V P and Kanatzidis M G 2014 *Energy Environ. Sci.* **7** 251
[4] Chang C, Wu M, He D, Pei Y, Wu C F, Wu X *et al* 2018 *Science* **360** 778
[5] Zhang Q, Liao B, Lan Y, Lukas K, Liu W, Esfarjani K *et al* 2013 *Proc. Natl. Acad. Sci. USA* **110** 13261
[6] Banik A, Shenoy U S, Saha S, Waghmare U V and Biswas K 2016 *J. Am. Chem. Soc.* **138** 13068
[7] Biswas K, He J, Zhang Q, Wang G, Uher C, Dravid V P *et al* 2011 *Nat. Chem.* **3** 160
[8] Biswas K, He J, Blum I D, Wu C I, Hogan T P, Seidman D N *et al* 2012 *Nature* **489** 414
[9] Jana M K and Biswas K 2018 *ACS Energy Lett.* **3** 1315
[10] Jana M K, Pal K, Waghmare U V and Biswas K 2016 *Angew. Chem. Int. Ed.* **55** 7792
[11] Guin S N, Pan J, Bhowmik A, Sanyal D, Waghmare U V and Biswas K 2014 *J. Am. Chem. Soc.* **136** 12712
[12] Roychowdhury S, Jana M K, Pan J, Guin S N, Sanyal D, Waghmare U V *et al* 2018 *Angew. Chem. Int. Ed.* **57** 4043
[13] Rathore E, Juneja R, Culver S P, Minafra N, Singh A K, Zeier W G *et al* 2019 *Chem. Mater.* **31** 2106
[14] Lee S, Esfarjani K, Luo T, Zhou J, Tian Z and Chen G 2014 *Nat. Commun.* **5** 3525
[15] Zhao L D, Lo S H, Zhang Y, Sun H, Tan G, Uher C *et al* 2014 *Nature* **508** 373
[16] Morelli D T, Jovovic V and Heremans J P 2008 *Phys. Rev. Lett.* **101** 35901
[17] Guin S N, Chatterjee A, Negi D S, Datta R and Biswas K 2013 *Energy Environ. Sci.* **6** 2603
[18] Wojciechowski K T and Schmidt M 2009 *Phys. Rev. B: Condens. Matter Mater. Phys.* **79** 184202
[19] Jovovic V and Heremans J P 2009 *J. Electron. Mater.* **38** 1504
[20] Pan L, Be D and Dragoe N 2013 *J. Am. Chem. Soc.* **135** 4914
[21] Guin S N, Srihari V and Biswas K 2015 *J. Mater. Chem. A* **3** 648
[22] Wu D, Pei Y, Wang Z, Wu H, Huang L, Zhao L D *et al* 2014 *Adv. Funct. Mater.* **24** 7763
[23] Rosi F D, Hockings E F and Lindenblad N E 1961 *RCA Rev.* **22** 82
[24] Xiao C, Qin X, Zhang J, An R, Xu J, Li K *et al* 2012 *J. Am. Chem. Soc.* **134** 18460
[25] Geller S and Wernick J H 1959 *Acta Crystallogr.* **12** 46
[26] Liu X, Jin D, Liang X, Liu X, Jin D and Liang X 2016 *Appl. Phys. Lett.* **109** 133901
[27] Wu H J, Wei P C, Cheng H Y, Deng J R and Chen Y Y 2017 *Acta Mater.* **141** 217
[28] Böcher F, Culver S P, Peilstöcker J, Weldert K S and Zeier W G 2017 *Dalton Trans.* **46** 3906
[29] Goto Y, Nishida A, Nishiate H, Murata M, Lee C H, Miura A *et al* 2018 *Dalton Trans.* **47** 2575
[30] Pei Y L, Wu H, Wu D, Zheng F and He J 2014 *J. Am. Chem. Soc.* **136** 13902
[31] Zebarjadi M, Joshi G, Zhu G, Yu B, Minnich A, Lan Y *et al* 2011 *Nano Lett.* **11** 2225
[32] Berry T, Fu C, Au G, Fecher G H, Schnelle W, Serrano-Sanchez F *et al* 2017 *Chem. Mater.* **29** 7042
[33] People R, Bean J C, Lang D V, Sergent A M, Störmer H L, Wecht K W *et al* 1984 *Appl. Phys. Lett.* **45** 1231
[34] Hasegawa Y, Ishikawa Y, Saso T, Shirai H, Morita H, Komine T *et al* 2006 *Physica B: Condens. Matter* **382** 140
[35] Gibson Q D, Schoop L M, Weber A P, Ji H, Perge S N, Drozdov I K *et al* 2013 *Phys. Rev. B* **88** 081108
[36] Valla T, Ji H, Schoop L M, Weber A P, Pan Z-H, Sadowski J T *et al* 2012 *Phys. Rev. B* **86** 241101